Electronic structure and energetics of ordered titanium carbides of composition Ti_2C

2002 J. Phys.: Condens. Matter 14 4425

(http://iopscience.iop.org/0953-8984/14/17/315)

INSTITUTE OF PHYSICS PUBLISHING JOURNAL OF PHYSICS: CONDENSED MATTER

J. Phys.: Condens. Matter **14** (2002) 4425–4444 PII: S0953-8984(02)31833-2

Electronic structure and energetics of ordered titanium carbides of composition Ti_2C

R Eibler

Institute of Physical Chemistry, University of Vienna, Währingerstraße 42, A-1090 Wien, Austria

E-mail: renate.eibler@univie.ac.at

Received 12 December 2001, in final form 22 March 2002
Published 18 April 2002
Online at stacks.iop.org/JPhysCM/14/4425

Abstract

The equilibrium geometries, formation energies, band structures, densities of states and charge densities of ordered titanium carbide phases of composition Ti_2C—cubic $Fd3m$-Ti_2C and trigonal $R\bar{3}m$-Ti_2C—were calculated self-consistently by means of the full-potential linearized augmented-plane-wave method. The trigonal phase was found to be more stable than the cubic phase by 11.6 kJ/(mole of atoms) because it enables more efficient d–d bonding between Ti d states. The cubic phase is stabilized by the relaxation of the Ti atoms next to the vacancies towards their nearest-neighbour C atoms. In agreement with experiment, the maximum of the stabilizing relaxation energy (2.8 kJ/(mole of atoms)) is found for a relaxation of 0.04 Å. The formation energies are in good agreement with the available experimental values for TiC and $Fd3m$-Ti_2C. Calculations were also performed for two tetragonal phases of composition Ti_2X found experimentally for the nitride but not for the carbide. All calculated ordered Ti_2C phases are found to be stable against segregation into TiC and metallic Ti.

1. Introduction

Owing to their hardness, high melting points and high stability, transition metal carbides and nitrides are widely used in industry. Because of their particular electronic structure they show an interesting combination of ionic, covalent and metallic properties. Non-stoichiometry is very common in these compounds. Their physical properties are significantly influenced by the amount of structural vacancies.

One of the most interesting systems is the titanium–carbon system. Titanium carbide crystallizes in the cubic sodium chloride (B1) structure within a broad homogeneity range (δ-TiC_x, $0.48 \leqslant x \leqslant 1.0$ [1, 2]) and with statistically distributed substitutional vacancies on the carbon sublattice sites. For a certain range of composition, the δ-phase seems to be thermodynamically stable solely at high temperatures. It can, however, be obtained quite easily as a metastable phase at lower temperatures by quenching the samples [3, 4].

At lower temperatures, ordered defect structures showing long-range order of the vacancies are the thermodynamically stable phases. They can, however, only be obtained after a special thermal treatment of the samples such as prolonged annealing [5, 6]. Because of the high migration enthalpy of the C vacancies (∼4 eV) [6] their formation is kinetically hindered at lower temperatures.

On the other hand, even in disordered TiC_x it can be concluded, e.g. from elastic diffuse neutron-scattering measurements [7–9], that the non-metal vacancies show some short-range order.

Long-range order in titanium carbide samples is, for instance, detected by additional superlattice reflections in x-ray and neutron diffraction [10], by different values for ordered and disordered phases of the electrical resistance [11–13], the specific heat [11] and other physical quantities and by characteristic jumps if one plots these quantities against the molar fraction x of the non-metal atoms [14].

One way of investigating theoretically the influence of vacancy ordering on the physical properties of TiC_x consists in the calculation of the electronic structure and energetics of the various ordered phases. Such calculations have already been performed; for example,

(a) by the recursion method with a parametrized tight-binding Hamiltonian for various possible ordered vacancy superstructures of transition metal carbides and nitrides [15];
(b) by the self-consistent tight-binding linear muffin-tin-orbital (TB-LMTO) method for ordered fcc $TiC_{0.25}$, $TiC_{0.5}$ and $TiC_{0.75}$ [16];
(c) by the self-consistent augmented-plane-wave (APW) method and the linearized muffin-tin atomic-sphere-approximation (LMTO-ASA) method for ordered fcc $TiC_{0.75}$ [17, 18];
(d) by a tight-binding parametrization for TiC_x ($0.7 \leqslant x \leqslant 1$) [19];
(e) very recently, by a combination of full-potential linear muffin-tin-orbital (FP-LMTO) and pseudopotential VASP calculations for various ordered TiC_x phases of cubic symmetry ($TiC_{0.25}$, $TiC_{0.5}$, $TiC_{0.625}$, $TiC_{0.75}$, $TiC_{0.875}$, $TiC_{0.9375}$, TiC), including a thorough consideration of relaxation effects [20].

For the related Ti–N system, *ab initio* self-consistent full-potential linearized augmented-plane-wave (FLAPW) band-structure calculations have been performed for experimentally observed ordered titanium nitride phases of composition Ti_2N with tetragonal symmetry: metastable δ'-Ti_2N (whose structure can be derived from the B1 structure by locating the vacancies at fixed non-metal lattice sites and relaxing the c/a ratio and the positions of the Ti atoms) and stable ϵ-Ti_2N crystallizing in the antirutile structure [21, 22].

In a preceding paper [22], the band structure of fictitious δ'-Ti_2C has been calculated as well. The comparison of the electron densities and the densities of states of δ'-Ti_2N and δ'-Ti_2C led to a qualitative explanation for the existence of the former and the non-existence of the latter phase in the respective phase diagrams. However, for the carbide the geometry optimization has not been performed.

It seemed of some interest to continue these investigations by performing band-structure calculations also for the experimentally found ordered cubic and trigonal Ti_2C phases. Moreover, the experimental evidence for the stabilities of these phases does not seem to have been conclusive until now and therefore additional theoretical calculations not restricted to cubic structures, such as [20], can be particularly helpful.

From TiC_x samples in the composition range $0.5 \leqslant x \leqslant 0.7$, two different ordered defect structures of the ideal composition Ti_2C have been identified experimentally: cubic Ti_2C of space group symmetry $Fd3m$ (No 227) [10] (figure 1) and trigonal Ti_2C of space group $R\bar{3}m$ (No 166) [23] (figure 2).

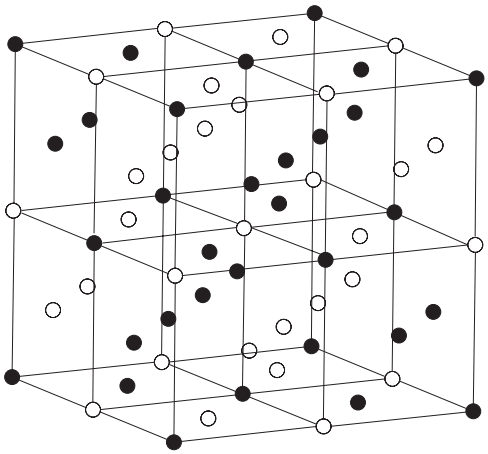

Figure 1. The cubic unit cell of $Fd3m$-Ti_2C drawn in a B1(NaCl)-type lattice. Full circles: C atoms; empty circles: vacancies. The Ti atoms are not shown.

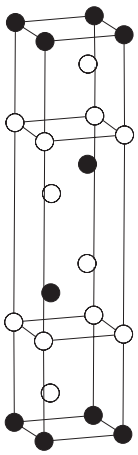

Figure 2. One third of a hexagonal unit cell of $R\bar{3}m$-Ti_2C. Full circles: C atoms; empty circles: Ti atoms.

Neglecting the trigonal distortion, the two structures have identical atomic distances and atomic pair correlations and, although they differ in their atomic arrangement [24, 25], they cannot be distinguished by means of x-ray or neutron powder diffraction.

In both structures, the C atoms and also the vacancies are surrounded by (distorted) Ti octahedra. As in short-range ordered TiC_x, the vacancies tend to avoid second-nearest C sublattice sites. The three nearest C neighbours of the Ti atoms are found in $+x$-, $+y$- and $+z$-directions. The structures can also be described by different stackings of octahedra centred at Ti atoms and consisting of C atoms and of C vacancies [6, 8].

The lattice parameter of cubic $Fd3m$-Ti_2C (Ti_2C (I)), with experimental values of 8.6 Å [10] and 8.54 Å [26], is twice as large as the lattice parameter of the B1 structure. The rhombohedral unit cell contains 12 atoms (four formula units of Ti_2C).

In $Fd3m$-Ti_2C, the filling of the C(111) planes alternates from 1/4 to 3/4 and the Ti atoms adjoining the vacancies are supposed to be shifted towards the C atoms by 0.04 Å [10].

For $R\bar{3}m$-Ti_2C, the C(111) planes are alternating between fully occupied or entirely unoccupied. The trigonal unit cell contains three atoms (one formula unit of Ti_2C). For this structure, however, it is also possible to construct a hexagonal unit cell which is three times as large accommodating three formula units of Ti_2C, i.e. nine atoms. Hexagonal lattice parameters of $a_{hex} = 3.06$ Å and $c_{hex} = 14.890$ Å were found for $TiC_{0.67}$ at 1003 K [9].

As regards the relative stabilities of these two structures, experimental results are not unambiguous. For a carbon content of $0.6 \leqslant x \leqslant 0.67$, de Novion [9] found the trigonal $R\bar{3}m$ phase to be the stable ordered phase above 973 K and the cubic $Fd3m$ phase a metastable, intermediately formed superstructure. For $x < 0.6$, at first cubic $Fd3m$-Ti_2C was formed from disordered TiC_x which transformed very slowly into $R\bar{3}m$-Ti_2C when the sample was isothermally annealed at 1003 K for more than one month [9]. Probably for kinetic reasons, the trigonal phase has not been obtained at lower temperatures.

Using high-resolution electron microscopy and the micro-diffraction technique, Tsurekawa and Yoshinaga [27] found a $R\bar{3}m$ superlattice for samples of $TiC_{0.59}$ annealed at 970 K for 140 h. Also Em and Tashmetov [28] found the trigonal phase to be stable below, and the cubic phase to be stable above 1053 K for samples of composition $TiC_{0.632}$.

According to investigations by Lipatnikov *et al* [14], vacancy ordering in the temperature range of 300–1100 K gave cubic $Fd3m$-Ti_2C for a C content of $0.52 \leqslant x \leqslant 0.55$ and trigonal $R\bar{3}m$-Ti_2C for a C content of $0.56 \leqslant x \leqslant 0.58$. For a C content of $0.62 \leqslant x \leqslant 0.68$, they identified a third ordered superstructure of composition Ti_3C_2 and with rhombic symmetry, which was first shown to exist by Khaenko *et al* [29].

Contrary to the case for the Ti–N system, no tetragonal phase of composition Ti_2C has been found in the temperature range investigated at and above 300 K. Gusev and Rempel [2] postulated a transition temperature below 300 K for a possible tetragonal δ'-Ti_2C. Altogether, no experimental information exists so far about the relative phase stabilities in the Ti–C system at low temperatures. Also, ordering of vacancies seems to be by no means perfect in the so-called ordered phases and impurities such as O or additional C atoms in a sample could stabilize or destabilize a particular phase.

When comparing the results of first-principles band-structure calculations with experimental findings it must always be taken into account that the former refer to a temperature of 0 K and are based on supercells with perfect stoichiometric composition and perfect long-range order of the vacancies but without any impurities.

2. Computational aspects

In the present *ab initio* study, band-structure calculations within the local-density approximation (LDA) of density-functional theory were performed by means of the FLAPW method [30] for cubic $Fd3m$-Ti_2C, for trigonal $R\bar{3}m$-Ti_2C and also for hypothetical tetragonal δ'-Ti_2C, ϵ-Ti_2C and $P4/mmm$-Ti_2C. The core states, including the Ti 3s and 3p states, were regarded as atomic-like and treated fully relativistically whereas the valence states were treated scalar relativistically. The wavefunctions were expanded into ≈140 augmented plane waves/atom with wavevectors up to $|\vec{k}| = 4.6$. Inside the muffin-tin spheres around the atomic sites the potentials and the charge densities were expanded in spherical harmonics up to $l = 8$. In the interstitial region the corresponding expansions were performed in Fourier series up to $|\vec{K}| = 10.00$. The muffin-tin radii were taken as 1.7322 au for C and 1.961 au for Ti.

A Hedin–Lundqvist exchange–correlation potential [31] was employed.

For the $\vec{k}$-integration the tetrahedron method [32] was used throughout. For the solutions of the Schrödinger equation 3600 $\vec{k}$-points in the Brillouin zone (BZ) for both cubic and trigonal Ti_2C were taken. This is equivalent to 300 $\vec{k}$-points in the irreducible wedge of the

BZ for $R\bar{3}m$-Ti_2C and to 75 $\vec{k}$-points for $Fd3m$-Ti_2C taking into account that the volume of the irreducible wedge of the BZ is 1/16 (1/48) of the entire BZ volume for the trigonal (cubic) structure. A mesh of 75 non-equivalent $\vec{k}$-points was employed for the tetragonal structures.

The influence of the number of $\vec{k}$-points on the results is rather small: increasing it from 75 to 300 for $R\bar{3}m$-Ti_2C changes the total energy only by 1 mRyd/formula unit. Thus, unlike in the FLAPW band-structure calculation for δ'-Ti_2N and ϵ-Ti_2N [22], no extrapolation to an infinite number of $\vec{k}$-points was undertaken.

An augmentation of the number of basis function lowers the total energy. However, for very large and thus overcomplete basis sets, numerical problems are to be expected. The chosen optimized cut-off value of $|\vec{k}_{max}| = 4.6$ was already tested successfully and applied in [22] and guarantees a sufficient convergence of the total energies (changes of <1 mRyd/atom if $|\vec{k}_{max}|$ is further increased).

The non-spherical terms of the Hamiltonian matrix were calculated for the full Hamiltonian. Compared to a calculation using the second variation method, the total energies are lowered by 2 mRyd/formula unit of Ti_2C at most and the equilibrium geometries slightly shifted ($<0.5\%$ deviation of the lattice parameters). No visible changes are found for the band structures, densities of states and charge densities.

The band-structure calculations for $Fd3m$-Ti_2C were performed both with and without empty spheres at the vacancy sites. This does not change the results significantly but, in the former case, allows for the localization of possible vacancy states as defined in [17].

In order to determine the optimized geometries and bulk moduli for all phases, the first step consisted in finding the minimum of the total energy with respect to the unit-cell volume by means of a Birch fit [33] where all other geometric parameters (c/a ratio for the trigonal and tetragonal phases, possible positional parameters and relaxations of the Ti atoms for the cubic $Fd3m$ phase and tetragonal δ'-phase) were fixed. In a second step, these other parameters were optimized at fixed equilibrium volume. Finally, the volume was once more varied with the fixed optimized values for these parameters.

3. Energetics

Figure 3 shows the total energies/formula unit as functions of the volume for $Fd3m$-Ti_2C (curve (b)) and $R\bar{3}m$-Ti_2C (curve (c)), whereby the other geometric parameters (c/a ratio for $R\bar{3}m$-Ti_2C, relaxation of the Ti atoms for $Fd3m$-Ti_2C) are fixed at the experimental values.

The equilibrium volume/formula unit of $Fd3m$-Ti_2C was found to be very near the experimental volume of 268.3 au^3 [10]. For $R\bar{3}m$-Ti_2C it lies 5.7% below the experimental value of 272.3 au^3 [9] and this volume contraction lowers the total energy of $R\bar{3}m$-Ti_2C by about 6 mRyd/formula unit. One must, however, take into account that the experimental value was determined for a carbide of composition $TiC_{0.67}$ at 1003 K [9], whereas the calculation was performed for perfectly ordered Ti_2C at 0 K.

Once the equilibrium volumes are determined, the influence on the total energy of the other geometric parameters can be studied.

Figure 4 shows the variation of the total energy of $Fd3m$-Ti_2C at the equilibrium volume with the relaxation of the Ti atoms next to the C vacancies. Zero relaxation here means that the Ti atoms are situated at the ideal positions of the fcc lattice. The outward relaxation of the Ti atoms from these positions towards their nearest C neighbours reduces the Ti–C bond length and lowers the total energy by 7 mRyd/formula unit. The theoretical value of 0.038 Å for the relaxation at the energy minimum is in excellent agreement with the experimental value of 0.04 Å [10].

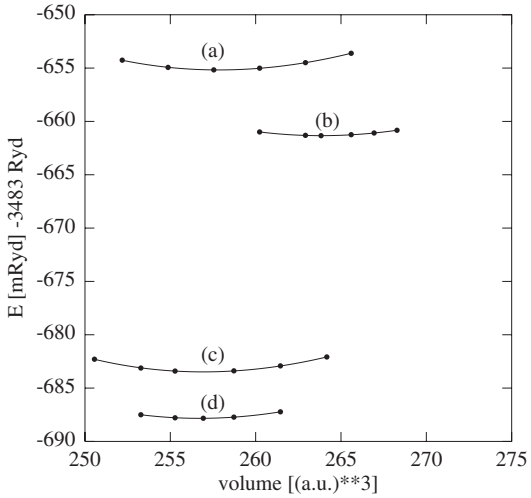

Figure 3. The volume dependence of the total energies/formula unit of $Fd3m$-Ti_2C and $R\bar{3}m$-Ti_2C: curve (a) unrelaxed $Fd3m$-Ti_2C; curve (b) relaxed $Fd3m$-Ti_2C; curve (c) $R\bar{3}m$-Ti_2C, experimental c/a ratio; curve (d) $R\bar{3}m$-Ti_2C, optimized c/a ratio.

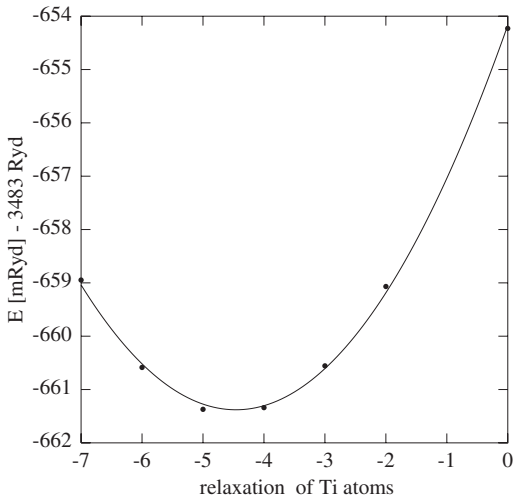

Figure 4. Total energy/formula unit of $Fd3m$-Ti_2C at equilibrium volume as function of the relaxation of the Ti atoms from the ideal fcc positions (in units of a thousandth of a lattice parameter).

Thus, curve (b) in figure 3 for the total energy of $Fd3m$-Ti_2C conforms already to the Birch fit with optimized equilibrium relaxation of the Ti atoms.

In order to take the influence of the Ti-atom relaxation on the total energy properly into account, a Birch fit was also performed for fictitious $Fd3m$-Ti_2C with unrelaxed Ti atoms at the fcc lattice positions (curve (a) in figure 3).

Relaxation was shown to increase the equilibrium volume by 2.3% and the relaxation energy, now defined as difference between the total-energy minima with and without relaxation of the Ti atoms, was determined as 6.2 mRyd/formula unit (2.1 mRyd/atom or 2.8 kJ/(mole of atoms)).

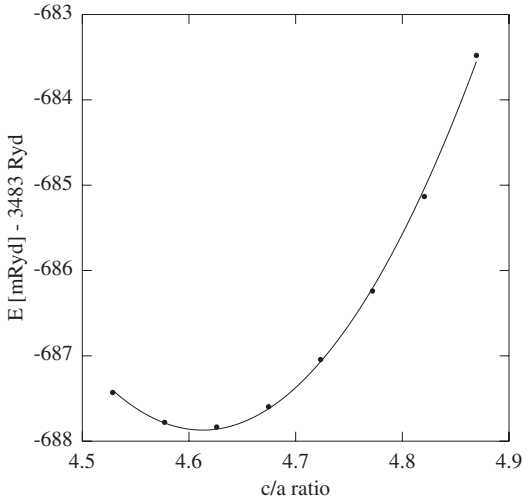

Figure 5. Total energy of $R\bar{3}m$-Ti_2C at equilibrium volume as a function of the c/a ratio.

Other experimental values for the outward relaxation of the Ti atoms bordering the vacancies in substoichiometric TiC_x are of the same order of magnitude: 0.03 Å for short-range ordered $TiC_{0.76}$ [34], 0.05 Å for $TiC_{0.64}$ and $TiC_{0.76}$ [35], 0.07 Å for ordered $TiC_{0.6}$ [36].

Previous calculations also found an outward relaxation of the Ti atoms but with slightly higher values. The FP-LMTO calculation [20] for the 16-atom supercell describing ordered Ti_2C and corresponding to the $Fd3m$ structure gave a Ti relaxation of 0.08 Å with a relaxation energy of 3 mRyd/atom whereby the equilibrium volume of the cell with relaxed Ti atoms is increased by 3% compared to the cell with unrelaxed Ti atoms. Cluster CNDO/2 calculations for an isolated C vacancy in TiC found a Ti relaxation of 0.107 Å [37] and a tight-binding parametrization led to a value of 0.1 Å for TiC_x ($0.7 \leqslant x \leqslant 1$) [19].

For $R\bar{3}m$-Ti_2C, the experimental positions of the Ti atoms are almost identical with their equilibrium positions, but a tetragonal distortion changing the c/a ratio can lower the total energy quite significantly. Figure 5 shows the variation of the total energy of $R\bar{3}m$-Ti_2C at fixed equilibrium volume with the c/a ratio. The energy minimum corresponding to a lowering of the total energy by 4.4 mRyd/formula unit was found for a c/a ratio which is 5% smaller compared to the experimental value measured for $TiC_{0.67}$ at 1003 K [9]. Therefore, a second volume minimization with the smaller c/a ratio was performed for $R\bar{3}m$-Ti_2C and the resulting Birch fit is shown as curve (d) in figure 3. The trigonal phase with the optimized c/a ratio is more stable by 26.5 mRyd/formula unit (11.6 kJ/(mole of atoms)) than the (relaxed) cubic $Fd3m$ phase.

For titanium nitride of composition $TiN_{0.5}$ two ordered phases of tetragonal symmetry exist, namely δ'-Ti_2N (space group $I4_1/amd$) [38] and ϵ-Ti_2C (space group $P4_2/mnm$; antirutile structure) [39]. The δ'-Ti_2N phase is metastable and transforms upon quenching to thermodynamically stable ϵ-Ti_2N. Its structure can be derived from the B1 structure by assuming a particular ordered arrangement of vacancies whereby each Ti atom is surrounded by three nearest non-metal neighbours. Unlike in the $Fd3m$ structure of Ti_2C these are, however, positioned in the $+x$-, $-x$- and z-directions. Therefore, relaxation of the Ti atoms is only possible in the z-direction. A detailed description of these structures can be found in [22], where the band structures and electron densities of δ'-Ti_2N and of fictitious δ'-Ti_2C have already been compared.

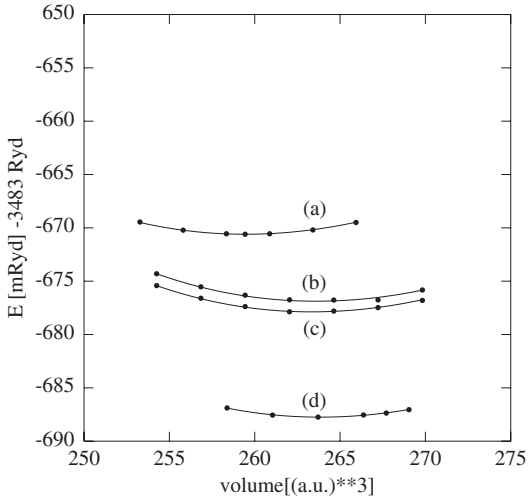

Figure 6. The volume dependence of the total energies/formula unit of δ'-Ti_2C and of ϵ-Ti_2C. Curve (a): unrelaxed δ'-Ti_2C with $c/a = 2$; curve (b): relaxed δ'-Ti_2C with $c/a = 2$; curve (c): relaxed δ'-Ti_2C with the optimized c/a ratio of 2.05; curve (d): ϵ-Ti_2C with the optimized c/a ratio.

The present study contains also a calculation of the energetics and equilibrium geometries of both fictitious δ'-Ti_2C and ϵ-Ti_2C which, probably for kinetic reasons [2], have not yet been traced experimentally.

Figure 6 shows calculated Birch fits for these two fictitious tetragonal phases. Curve (a) corresponds to ordered $TiC_{0.5}$ with $c/a = 2$ and unrelaxed Ti atoms. If the Ti atoms are relaxed at the equilibrium volume, an optimized relaxation value of 0.03 Å results. The Birch fit for δ'-Ti_2C with this relaxation value but still with $c/a = 2$ is shown as curve (b). Finally, curve (c) refers to relaxed δ'-Ti_2C with the optimized c/a ratio of 2.05. Curve (d) shows the Birch fit of ϵ-Ti_2C with the optimized c/a ratio.

For δ'-Ti_2C with $c/a = 2$ almost the same value of the relaxation energy as for $Fd3m$-Ti_2C—namely 6.2 mRyd/formula unit (2.1 mRyd/atom, 2.8 kJ/(mole of atoms))—is found, which can be compared to the higher value of 5.1 kJ/(mole of atoms) for the relaxation energy of δ'-Ti_2N with $c/a = 2$ [22]. The energy gain by a tetragonal distortion changing the c/a ratio is for the carbide with 0.3 mRyd/atom much smaller than the value of 1.9 mRyd/atom for the nitride. Relaxation and tetragonal distortion stabilize δ'-Ti_2N by 5.3 mRyd/atom (7 kJ/(mole of atoms)) [22] and δ'-Ti_2C by only 2.4 mRyd/atom (3.2 kJ/(mole of atoms)). The energy of transformation of the δ'-phase to the ϵ-phase amounts to 3.4 mRyd/atom (4.5 kJ/(mole of atoms)) for the carbide and to 2.4 mRyd/atom (3.1 kJ/(mole of atoms)) for the nitride [22].

Although neither tetragonal phases has yet been found experimentally, the present calculation shows them to be more stable than $Fd3m$-Ti_2C and, in the case of ϵ-Ti_2C, even as stable as trigonal $R\bar{3}m$-Ti_2C.

However, these results reflect only the relative thermodynamic stabilities at 0 K for the ideal composition of $TiC_{0.5}$ (and, in the case of $Fd3m$-Ti_2C and of δ'-Ti_2C, for perfectly ordered vacancies). Neither entropic contributions to the Gibbs energies at non-zero temperatures nor the influence of possible remaining disorder and of deviations from the exact stoichiometric composition are taken into account.

Also, a high value of the free activation energy for the phase transition excludes the formation of a phase which is only stable at low temperatures (as was indeed postulated for

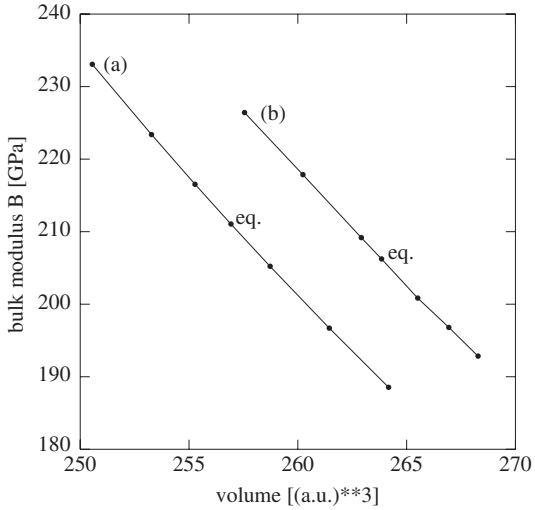

Figure 7. The volume dependence of the bulk moduli of (a) $R\bar{3}m$-Ti_2C and (b) $Fd3m$-Ti_2C. The bulk moduli at the equilibrium volume are labelled.

δ'-Ti_2C [2]). In short-range ordered fcc TiC_x, the C vacancies avoid second-nearest C sublattice sites [9]. Therefore, the formation of the δ'-structure, which also comprises C vacancies at second-nearest C sublattice sites was found to be unlikely too. The $Fd3m$ structure with an arrangement of vacancies compatible with the preferred vacancy sites found for short-range ordered TiC_x can be expected to be more easily formed. From our calculation, it should transform to thermodynamically much more stable $R\bar{3}m$-Ti_2C after trigonal distortion. However, experimental evidence suggests that this transformation will only take place if the temperature is high enough to surmount the activation energy for the transformation.

The calculated experimental and calculated equilibrium geometries for all phases together with the corresponding formation energies per atom and the bulk moduli B_0 at the equilibrium geometry can be found in table 1. Where available the theoretical FP-LMTO values of [20] are also given. Also included are the formation energies for the segregated phase (TiC and metallic Ti) and for stoichiometric TiC.

The formation energies per atom (for 0 K) were calculated from

$$E_{form} = \frac{E(\mathrm{Ti}_m\mathrm{C}_n) - mE(\mathrm{Ti}_{\mathrm{hcp}}) - nE(\mathrm{C}_{\mathrm{graphite}})}{n+m}. \tag{1}$$

They agree within 10% with the values of [20]. All ordered structures of composition Ti_2C were found to be less stable than stoichiometric TiC but all are stable against segregation into TiC and metallic Ti.

Experimentally, the formation energy $\Delta^0 H$ of TiC at room temperature was found as 92.1 kJ/(mole of atoms) [41] compared to our value of 93.1 kJ/(mole of atoms) at 0 K. The experimental estimate for $\Delta^0 H$ of $Fd3m$-Ti_2C at room temperature lies at 64 kJ/(mole of atoms) [42] compared to our values of 66.7 kJ/(mole of atoms) for unrelaxed and of 69.4 kJ/(mole of atoms) for relaxed $Fd3m$-Ti_2C.

The bulk moduli of the different Ti_2C phases were determined from the Birch fits. They agree well with the calculated value of 204 GPa for ordered Ti_2C from [20] and, as expected, lie below the experimental value of 242 GPa for $TiC_{0.91}$ [43]. In accordance with a comparable FLAPW calculation [44], the bulk moduli decrease with increasing volume (figure 7).

Table 1. Experimental and equilibrium lattice parameters (Å), formation energies per atom (mRyd) and bulk moduli B_0 (GPa) at the equilibrium geometry.

Phase	a_{eq}	a_{exp}	c_{eq}	c_{exp}	E_{form}	B_0
$Fd3m$-Ti_2	8.49	—	—	—	−50.8	208
unrelaxed	8.41 [20]				−46.7 [20]	213 [20]
$Fd3m$-Ti_2C	8.55	8.60 [10]	—	—	−52.9	207
relaxed	8.50 [20]	8.58 [26]			−49.7 [20]	204 [20]
$R\bar{3}m$-Ti_2C	3.05	3.06 [9]	14.13	14.91 [9]	−61.7	211
'δ'-Ti_2C', $c/a = 2$, unrelaxed	4.25	—	8.50	—	−56.0	212
'δ'-Ti_2C', $c/a = 2$, relaxed	4.28	—	8.56	—	−58.1	216
'δ'-Ti_2C', $c/a = 2.05$, relaxed	4.24	—	8.90	—	−58.4	218
'ϵ-Ti_2C'	5.03	—	3.09	—	−61.7	213
TiC + Ti (segregation)	—	—	—	—	−47.3	
B1-TiC	4.32	4.33 [40]	—	—	−70.9	240
	4.27 [20]				−65.8 [20]	278 [20]

In this calculation a higher value of 286 GPa was found for the bulk modulus of stoichiometric TiC and a decrease of the bulk moduli with an increasing number of vacancies for VC and $VC_{0.75}$ [44].

The features of the band structures, densities of states and electron densities which could explain the results for the energetics of Ti_2C will be discussed in the following sections.

4. Band structures and densities of states

Figure 8 shows, for $Fd3m$-Ti_2C (four formula units of Ti_2C) in its equilibrium geometry: (*a*) the band structure in several symmetry directions of the BZ; (*b*) the density of states (DOS) with and without relaxation of the Ti atoms; (*c*) the partial local Ti d and C s and p DOS; and (*d*) the partial local vacancy s and p DOS.

The four lowest bands originating from atomic C s states are separated by a gap of 4.4 eV from the higher bands formed from C p states. Interaction of C s and Ti d states is only found for the two upper, almost degenerate C s bands which are extremely flat and lead to an extremely high and narrow DOS peak at the top of the DOS 's band' region from −11.2 eV to −9.6 eV. The DOS for the C s bands with its three distinct maxima shows more structure than is usually found for transition metal carbides or nitrides.

The next occupied energy states produce three distinct DOS peaks which are separated from each other by narrow pseudogaps. Further analysis of the large components of the partial local DOS, namely the C s and p and Ti d DOS (figure 8(*c*)), shows that the first two peaks, designated as peaks p1 and p2 in figure 8(*b*), originate from interacting C p and Ti d

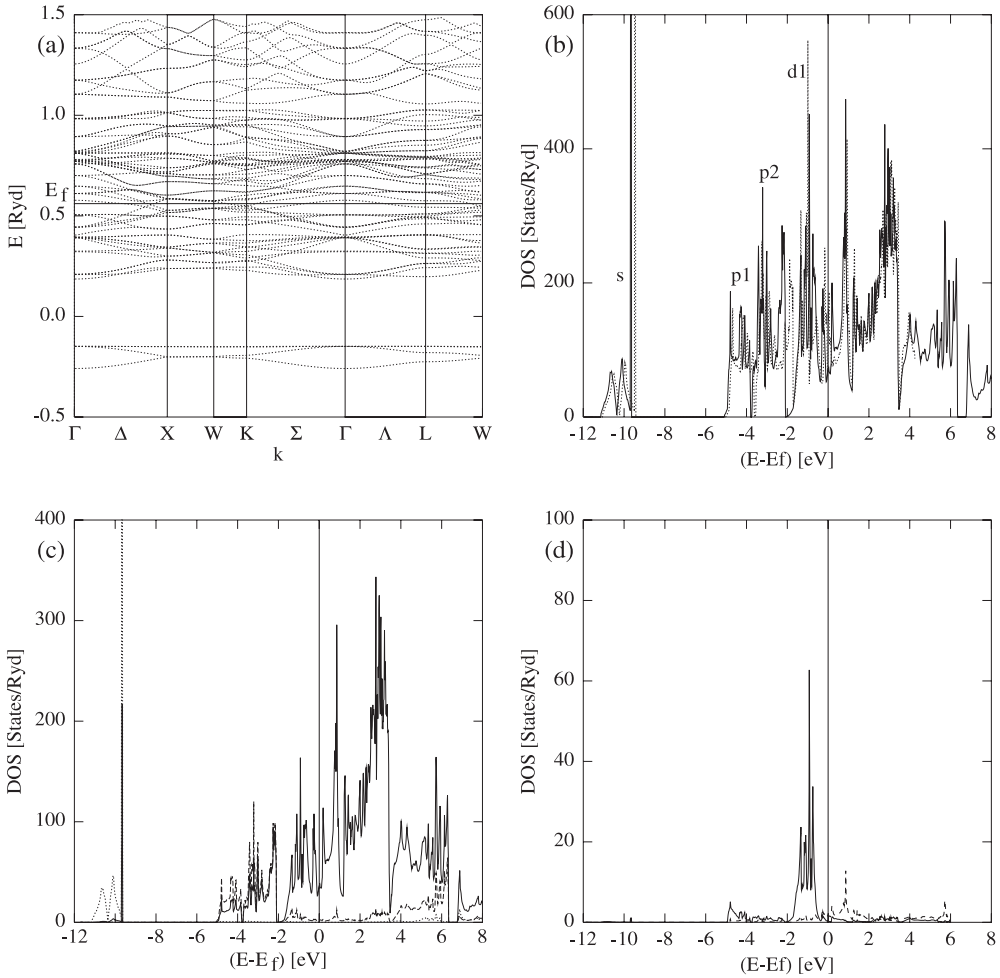

Figure 8. $Fd3m$-Ti_2C: (*a*) band structure in several symmetry directions; (*b*) DOS of $Fd3m$-Ti_2C with (full curve) and without (dashed curve) relaxation of the Ti atoms with respect to the fcc lattice positions; (*c*) partial local Ti d (full curve), C p (dashed curve) and C s (dotted curve) DOS; (*d*) partial local vacancy s (full curve) and p (dashed curve) DOS.

states whereas the third peak, designated as peak d1, can be associated with interacting Ti d states. The Fermi level is situated in a minimum between two narrow peaks which have predominantly Ti d character. Their energy distance is only 0.41 eV. Thus, any deviation from the stoichiometric composition should destabilize this structure.

The dotted and dashed curves in figure 8(*d*) are the partial local vacancy s and p DOS which have been determined by using empty spheres at the vacancy lattice sites. The partial vacancy s DOS has its maximum at approximately 1 eV below the Fermi level in peak d1. It can be ascribed to *vacancy states* which were found for substoichiometric titanium carbides in earlier calculations [16, 17] and also in XPS spectra [16].

The band structure and DOS were also calculated for fictitious unrelaxed $Fd3m$-Ti_2C with the Ti atoms at the fcc lattice positions. In this case, the Fermi level is found in a DOS maximum. Only if the Ti atoms are allowed to relax away from the vacancies is the Fermi

level shifted to a DOS minimum generated by the split of this DOS peak into two subpeaks (see figure 8(*b*)).

Relaxation also causes a sharper structure of the DOS and a shift of all bands towards lower energies. This is true particularly for the states at the top of the peak p2. As a consequence, the pseudogap between this peak and peak d1 is only found for $Fd3m$-Ti_2C with relaxed Ti atoms. Thus, from the effects of the Ti relaxation on the DOS, a qualitative explanation for its stabilizing effect can be given in addition to the quantitative result of a total-energy reduction by 2.1 mRyd/atom for a relaxation by 0.04 Å with respect to the ideal positions in the fcc lattice.

The partial local DOS for $Fd3m$-Ti_2C (see figure 8(*c*)) are in good agreement with the FP-LMTO partial local DOS for Ti_2C [20]. The 16-atom supercell for Ti_2C [20] corresponds to the unit cell of the $Fd3m$ structure. Relaxation effects on the partial local DOS also compare well in the two *ab initio* calculations.

Agreement is not so good with the tight-binding LMTO DOS for Ti_2C [16], probably because it was calculated for a different ordered defect structure. In [16], the $P4/mmm$ CuAu structure is assumed for Ti_2C. It is based on an fcc unit cell with alternating occupied or empty C layers in the [001] direction. However, the formation of this structure is highly improbable for a non-stoichiometric carbide because it would comprise an inhomogeneous distribution of the vacancies where the Ti atoms are surrounded by four vacancies and only two C atoms as nearest neighbours. From experiment, defect structures with a uniform distribution of vacancies are energetically favoured for substoichiometric transition metal carbides and nitrides [4, 20]. Moreover, in the CuAu structure there is no possibility for the Ti atoms to relax.

Inspection of the calculated DOS shows that the Fermi level is situated in a DOS maximum. The formation energy of this structure is calculated as −51.4 mRyd/atom and from table 1 its value lies 1.5 mRyd/atom below the value for relaxed $Fd3m$-Ti_2C.

Figure 9 shows for $R\bar{3}m$-Ti_2C in its equilibrium geometry: (*a*) the band structure; (*b*) the DOS; and (*c*) the partial local Ti d and C s and p DOS. The band structure is plotted for the hexagonal unit cell accommodating three formula units of Ti_2C. The three overlapping C s bands produce a single peak in the DOS. As for $Fd3m$-Ti_2C, only the C s states at the top of the peak interact with Ti d states. Again, two subpeaks p1 and p2 can be seen in the 'p band' region of the DOS but a gap of 0.1 eV now separates the upper peak p2 from the lowest occupied Ti 'd band' peak d1. The pseudogap between the peaks originating from occupied and unoccupied Ti d states is much wider than for $Fd3m$-Ti_2C, mainly because the small DOS side-peak at 0.2 eV below E_F for $Fd3m$-Ti_2C is shifted, for $R\bar{3}m$-Ti_2C, to 0.6 eV below E_F (and to 1 eV below the lowest DOS peak of unoccupied Ti d states).

The dotted curve in figure 9(*b*) represents the DOS of $R\bar{3}m$-Ti_2C for the experimental geometry. All peaks are shifted to higher energies. The bandwidth of the upper 'p band' peak p2 has increased and thus only a narrow pseudogap persists between peaks p2 and d1.

Comparison of $R\bar{3}m$- and $Fd3m$-Ti_2C shows that the s–p gap of $R\bar{3}m$-Ti_2C is narrower by 0.7 eV, shifting the bottom of peak p1 by 0.7 eV to lower energies. The larger separation of the two 'p band' subpeaks p1 and p2 in this compound increases the total width of the 'p band' by 0.6 eV. However, a true gap of 0.1 eV between peaks p2 and d1 remains. Additionally, peak d1 for occupied Ti 3d states narrows by 0.1 eV. These differences in the DOS can explain in a qualitative way the higher thermodynamic stability of $R\bar{3}m$-Ti_2C.

The densities of states for the fictitious phases δ'-Ti_2C and ϵ-Ti_2C are presented in figure 10.

For both structures the Fermi level lies in the lowest peak of interacting Ti 3d states which is separated only by a pseudogap from the 'p band' region of the DOS. The split of the DOS in this region into two separate peaks is less pronounced, especially for δ'-Ti_2C. The DOS of disordered $TiC_{0.5}$ which was calculated by means of the KKR-CPA method [45] shows the

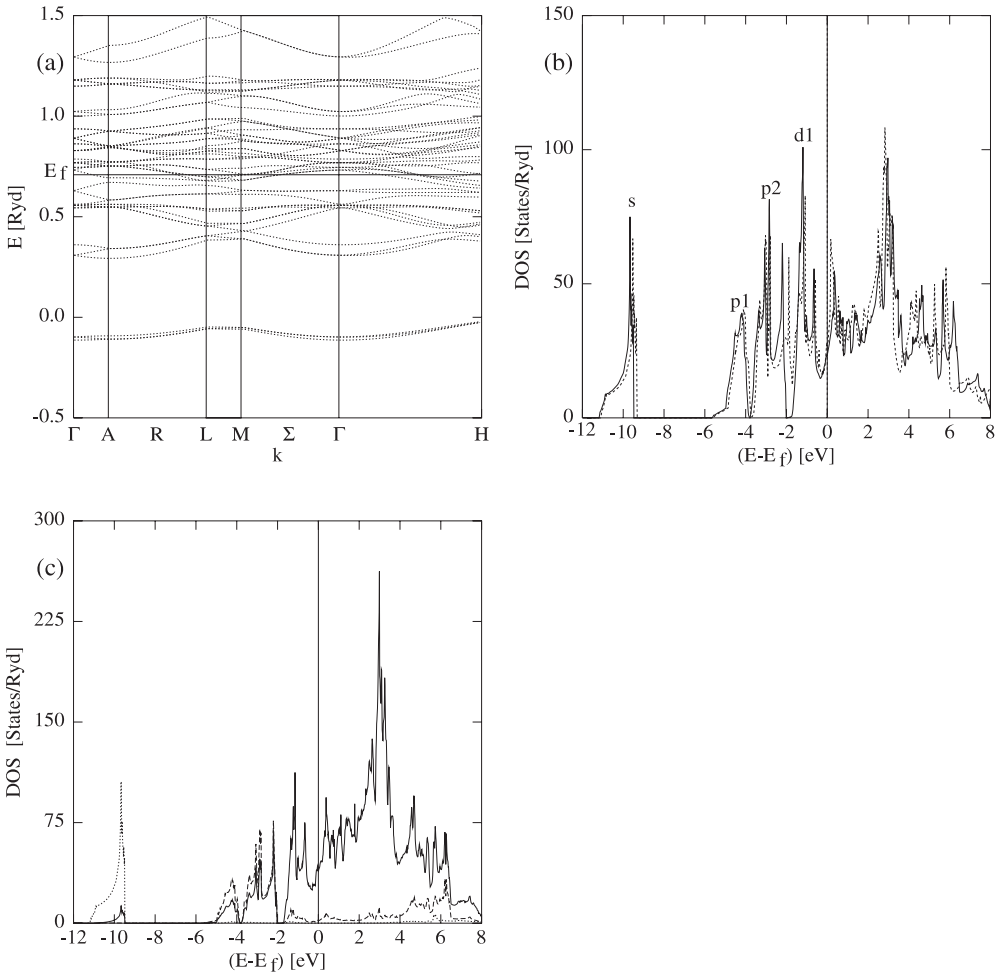

Figure 9. $R\bar{3}m$-Ti_2C: (*a*) band structure in several symmetry directions; (*b*) DOS for the equilibrium (full curve) and the experimental (dashed curve) geometry; (*c*) partial local Ti d (full curve), C s (dotted curve) and C p (dashed curve) DOS.

same features as the DOS of these two fictitious phases but the peaks are broadened by the disorder.

In order to facilitate comparison, all relevant bandwidths and band gaps can be found in table 2.

5. Electron densities

Contour plots of the valence electron density can help to visualize the nature of chemical bonding in solids.

Figure 11 shows, for $Fd3m$-Ti_2C in its equilibrium geometry, contour plots in the (100) plane of: (*a*) the total valence electron density; (*b*) the d1, (*c*) the p1 and (*d*) the p2 subpeak valence electron density. The latter are found by addition of the valence-electron-density contributions of all states with energies in the range of the respective DOS subpeaks (figure 8(*b*)).

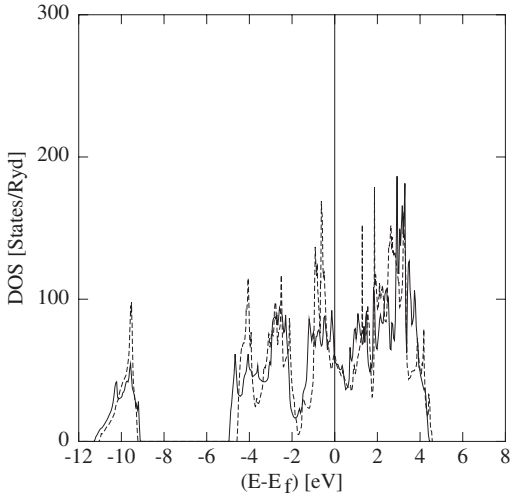

Figure 10. DOS of fictitious δ'-Ti_2C (full curve) and fictitious ϵ-Ti_2C (dashed curve).

Table 2. Calculated bandwidths and band gaps (in eV) for several Ti_2C phases. The band bottoms are given with respect to E_F.

	$Fd3m$-Ti_2C	$R\bar{3}m$-Ti_2C	δ'-Ti_2C	ϵ-Ti_2C	$TiC_{0.5}$ [45]
C 's band' width	1.6	1.7	2.2	1.9	
Bottom of C 's band'	−11.2	−11.2	−11.3	−11.1	
s–p gap	4.4	3.8	3.7	4.2	4.6
C 'p band' width	3.0	3.6	3.3	2.8	3.5
Bottom of C 'p band'	−5.0	−5.7	−5.0	−4.6	−5.2
p–d gap	—	0.1	—	—	—
Bottom of Ti 'd band'	−2.0	−1.9	−1.7	−1.8	−1.6

The (100) contour plot of the total valence electron density (figure 11(a)) shows the individual Ti_2C units to be interconnected by strong Ti d–C p bonds, forming strings consisting of a C layer with Ti layers above and below. The strings are separated from each other by an empty layer originating from the vacancies on the C lattice sites. In the strings, the C atoms are surrounded by octahedra of Ti atoms, which are slightly distorted because of the relaxation of the Ti atoms.

How do the states in different energy regions contribute to the total valence electron density? From figures 11(b)–(d), states in the energy region of the DOS subpeak p1 mainly form C p–p σ-bonds (figure 11(c)) and those of peak p2 mainly form σ-bonds between C p and Ti d states of t_{2g} symmetry (figure 11(d)). The Ti e_g-like states in the subpeak d1 just below E_F interact with each other and form Ti d–d bonds (figure 11(b)).

It is also enlightening to plot contributions of particular states to the valence electron density.

Thus, figure 12 shows (100) contour plots of three states of $Fd3m$-Ti_2C at $\vec{k} = \Gamma$ which represent different bonding types. The valence-electron-density contour plot for the state with energy $E = 0.186$ Ryd situated in the subpeak p1 (figure 12(a)) shows a typical C p–p σ-bond, the contour plot of the state with energy $E = 0.3925$ Ryd situated in the subband p2 (figure 12(b)) shows a bond between Ti t_{2g} and C p states and, finally, in the contour plot of the state with energy $E = 0.5048$ Ryd in band d1 just below E_F (figure 12(c)), the Ti t_{2g}-like

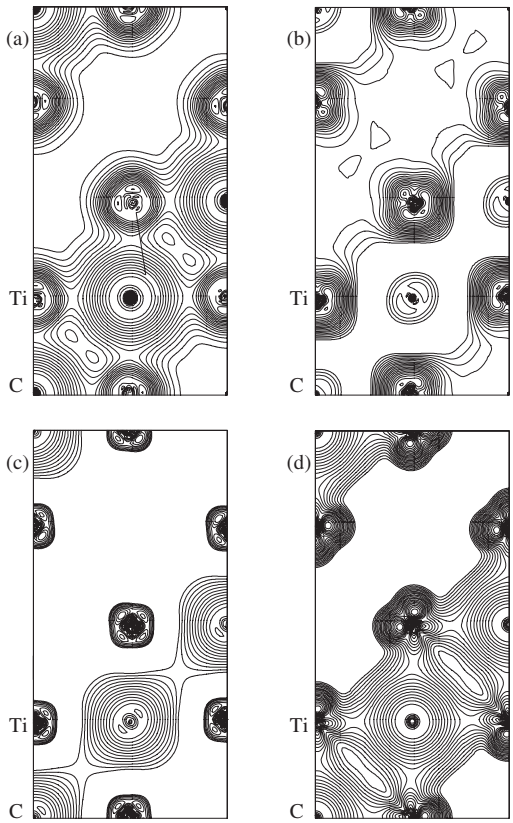

Figure 11. $Fd3m$-Ti_2C: contour plots in the (100) plane of (*a*) the total valence electron density, (*b*) the d1, (*c*) the p1 and (*d*) the p2 subband valence electron densities. For the definition of the subbands, see figure 8(*b*). The contour lines of figures 11, 13 and 14 are in units of e Å^{-3} on a logarithmic mesh starting with a value of 0.0625.

states are seen to form mutual d–d bonds and also bonds across the C vacancy. Thus, this last state can be described as a *vacancy state* in a real crystal and its contour plot can be compared to those already published for compounds such as fictitious $TiC_{0.75}$ [17], δ'-Ti_2N [21] and fictitious $TiO_{0.75}$ [46].

Figure 13 shows the total valence electron density of $R\bar{3}m$-Ti_2C at the equilibrium geometry. Based on the hexagonal unit cell, contour plots in three different planes were calculated: in the (100) plane (figure 13(*a*)); in the (001) plane with $z = 0$ (C layer) (figure 13(*c*)); and in the (001) plane with $z = 2.23$ (Ti layer) (figure 13(*d*)). Figure 13(*b*) shows the contour plot in the (100) plane for the geometry with the equilibrium volume but the experimental c/a ratio.

In the (100) contour plots (figures 13(*a*) and (*b*)), the Ti_2C units are seen to form a layer structure with three layers of Ti, C and Ti atoms, which are separated by an empty layer from the next Ti–C–Ti layer sequence. The individual Ti_2C units joined by C p–Ti d bonds are connected with each other by Ti d–d bonds between t_{2g} states located at Ti atoms in different Ti layers.

The C atoms in the C-atom layer (figure 13(*c*)) are close packed and connected by C p–p σ-bonds. Their electron density is almost spherical.

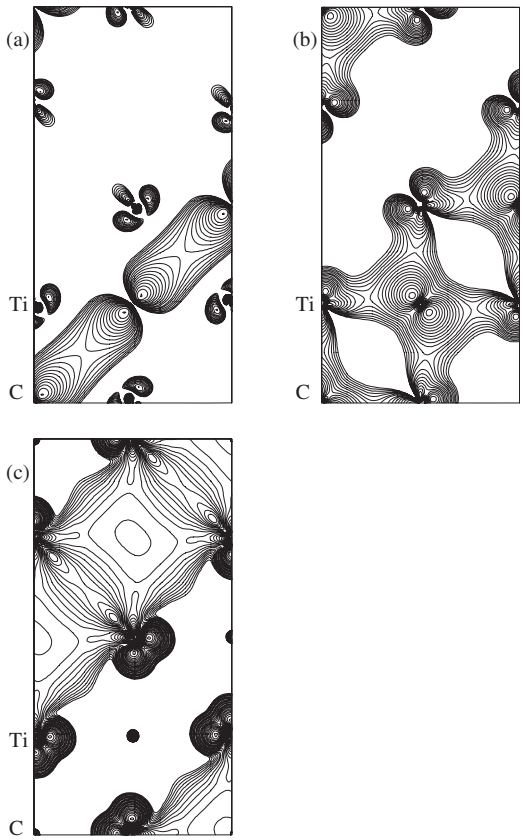

Figure 12. $Fd3m$-Ti_2C: contour lines in the (100) plane of the valence electron density of the states at $\vec{k} = \Gamma$ with energy (*a*) $E = 0.186$ Ryd, (*b*) $E = 0.3925$ Ryd and (*c*) $E = 0.5048$ Ryd. The contour lines of figures 12 and 15 are in units of e Å^{-3} on a logarithmic mesh starting with a value of 0.007 81.

More information about the states involved in the different bonding types can again be obtained by plotting the valence-electron-density contributions in a particular energy range.

Referring to figure 9(*b*) for the definition of the DOS subpeaks, the valence electron density of the states in subpeak p1 shows no bonding in the (100) plane. These states of predominantly C p character form, however, bonds in the C layer (figures 14(*a*) and (*d*)).

The C p states in the DOS subpeak p2 are both involved in interlayer p–d bonding with Ti t_{2g} states (figure 14(*b*)) and in intralayer C p–p bonding in the (001) plane (figure 14(*e*)). The Ti t_{2g} states in this energy range form also interlayer and intralayer Ti d–d bonds but only with Ti atoms in the same string (figures 14(*b*) and (*f*)).

On the other hand, the Ti d states of subpeak d1 interact in order to form both intralayer Ti d–d bonds in the (001) plane and also interlayer Ti d–d bonds in the (100) plane with Ti atoms of the adjoining Ti layer belonging to another string (figures 14(*c*) and (*g*)). They are thus responsible for the connection between the strings. The delocalized character of these bonds stabilizes the d states and lowers their energy more than is the case for the d states in the d1 peak of $Fd3m$-Ti_2C (compare the DOS plots for the two structures (figures 8(*b*) and 9(*b*))). This could also be a possible explanation for the higher stability of $R\bar{3}m$-Ti_2C compared with $Fd3m$-Ti_2C.

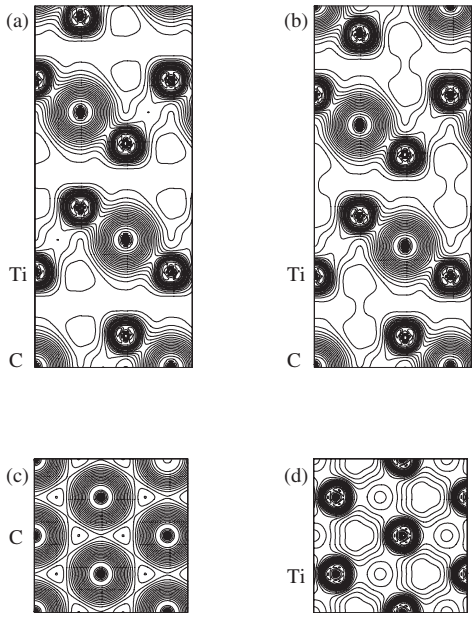

Figure 13. The valence electron density of $R\bar{3}m$-Ti_2C: in the (100) plane, calculated (*a*) without and (*b*) with relaxation of the c/a ratio; and for a C layer (*c*) and a Ti layer (*d*) in the (001) plane calculated with the relaxed c/a ratio. The sections in figures 13–15 relate to the hexagonal unit cell.

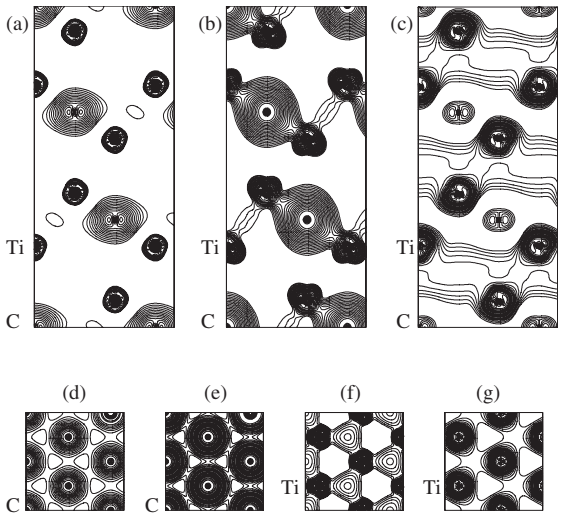

Figure 14. $R\bar{3}m$-Ti_2C at the equilibrium geometry: contour plots of the (*a*) p1, (*b*) p2 and (*c*) d1 subband valence electron densities in the (100) plane; of the (*d*) p1 and (*e*) p2 subband valence electron densities for a C layer in the (001) plane; of the (*f*) p2 and (*g*) d1 subband valence electron densities for a Ti layer in the (001) plane. For the definition of the subbands, see figure 9(*b*).

Charge-density contours for individual states of $R\bar{3}m$-Ti_2C are plotted in figure 15. The state at $\vec{k} = \Gamma$ with energy $E = 0.3082$ Ryd and thus situated in subband p1 (figure 15(*a*)) is a typical C p–p bonding state. The (100) contour plot of the Δ state at $\vec{k} = (001/4)$ in subpeak

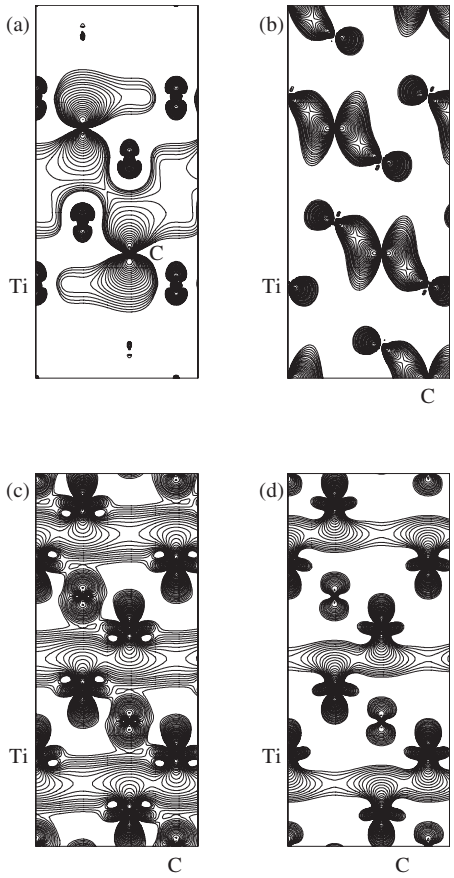

Figure 15. $R\bar{3}m$-Ti_2C at the equilibrium geometry: valence electron density in the (100) plane for (*a*) the Γ state with $E = 0.3282$ Ryd; (*b*) the Δ state with $E = 0.5447$ Ryd; (*c*) the Γ state with $E = 0.6289$ Ryd; (*d*) the Δ state with $E = 0.6534$ Ryd.

p2 with energy $E = 0.5447$ Ryd shows C p–Ti d σ-bonding (figure 15(*b*)), whereas the Γ state with energy $E = 0.6289$ Ryd in subpeak d1 shows delocalized Ti d–d bonds as well as some bonding of the Ti e_g-like states with C p states (figure 15(*c*)). This latter bonding type is not found for the Δ 'd band' state at $\vec{k} = (00\frac{1}{4})$ with energy $E = 0.6534$ Ryd (figure 15(*d*)).

6. Conclusions

From the present first-principles band-structure calculations, conclusions can be drawn about the relative thermodynamic phase stabilities of ordered phases of composition $TiC_{0.5}$ at 0 K where no experimental data are available. The thermodynamically stable phase at 0 K for the ideal composition Ti_2C is found to be the trigonal phase with $R\bar{3}m$ symmetry. Its equilibrium volume and c/a ratio are smaller by 5.7 and 5%, respectively, than the experimental values, which were, however, determined for $TiC_{0.67}$ at 1103 K [9]. The volume contraction reduces its total energy by 2.6 kJ/(mole of atoms) and the reduction of the c/a ratio by a further 1.9 kJ/(mole of atoms). The phase is seen to be stabilized by efficient d–d bonding of Ti atoms across the empty C sublayers.

The phase transformation energy defined as the difference of the total energies of $R3m$-Ti_2C in its equilibrium geometry and cubic, relaxed $Fd3m$-Ti_2C amounts to 11.6 kJ/(mole of atoms).

The latter phase is stabilized by the relaxation of the Ti atoms from the atomic positions in the fcc lattice towards their nearest C neighbours. This relaxation brings about a strengthening of C p–Ti d bonds but also a certain weakening of Ti d–d bonding. The maximum of the stabilization energy, namely 2.8 kJ/(mole of atoms), is found for the experimental relaxation value of 0.04 Å.

The present calculation indicates $R\bar{3}m$-Ti_2C to be the phase thermodynamically more stable than $Fd3m$-Ti_2C if the situation at 0 K is considered for the ideal composition of Ti_2C without any remaining disorder. It cannot give an answer to the question of which phase will actually be formed under experimental, and thus different, conditions. For this purpose, further theoretical research concerning the kinetics of phase transformation should be undertaken which would require, e.g., the calculation of activation barriers for the transformation from the cubic into the trigonal phase in order to follow the course of the total energies along the transformation path.

From our calculations, tetragonal ϵ-Ti_2C should be thermodynamically as stable as trigonal $R\bar{3}m$-Ti_2C at 0 K. As regards the ordered defect structures based on the fcc lattice of B1-TiC_x, δ'-Ti_2C should be more stable than $Fd3m$-Ti_2C. These tetragonal phases cannot be traced experimentally because they seem to be stable only at low temperatures [2] where their formation is kinetically hindered and where no experimental phase-diagram data are available.

Fictitious $P4/mmm$-Ti_2C is less stable than relaxed $Fd3m$-Ti_2C and the other calculated Ti_2C phases.

From the calculated formation energies which are in good agreement with experimental values [41,42] all calculated Ti_2C phases are stable against segregation into TiC and metallic Ti.

Acknowledgment

Thanks are due to Peter Herzig for his comments on the manuscript.

References

[1] Toth L E 1971 *Transition Metal Carbides and Nitrides* (New York: Academic)
[2] Gusev A I and Rempel A A 1997 *Phys. Status Solidi* a **163** 273
[3] Gusev A I 1991 *Phys. Status Solidi* b **163** 17
[4] Gusev A I and Rempel A A 1993 *Phys. Status Solidi* a **135** 15
[5] de Novion C H and Maurice V 1977 *J. Physique Coll.* **7** 211
[6] de Novion C H and Landesman J P 1985 *Pure Appl. Chem.* **57** 1391
[7] Billingham J, Bell P S and Lewis M H 1972 *Acta Crystallogr.* A **28** 602
[8] Sauvage M and Parthé E 1972 *Acta Crystallogr.* A **28** 607
[9] de Novion C H, Beuneu B, Priem T, Lorenzelli N and Finel A 1990 *The Physics and Chemistry of Carbides, Nitrides and Borides (NATO ASI Series E, vol 185)* (Dordrecht: Kluwer) p 329
[10] Goretzki H 1967 *Phys. Status Solidi* **20** K141
[11] Lorenzelli N, Caudron R, Landesman J P and de Novion C H 1986 *Solid State Commun.* **59** 765
[12] Vlasov V A, Karimov Yu S and Kustova L V 1986 *Izv. Akad. Nauk SSSR Neorg. Mater.* **22** 231
[13] Emel'yanov A N 1996 *Phys. Solid State* **38** 2003
[14] Lipatnikov V N, Kottar A, Zueva V and Gusev A I 1998 *Phys. Solid State* **40** 1211
[15] Landesman J P, Tréglia G, Turchi P and Ducastelle F 1985 *J. Physique* **46** 1001
[16] Guemmaz M, Moraitis G, Mosser A, Khan M A and Parlebas J C 1997 *J. Electron Spectrosc. Relat. Phenom.* **83** 173
[17] Redinger J, Eibler R, Herzig P, Neckel A, Podloucky R and Wimmer E 1985 *J. Phys. Chem. Solids* **46** 383
Redinger J, Eibler R, Herzig P, Neckel A, Podloucky R and Wimmer E 1986 *J. Phys. Chem. Solids* **47** 387

[18] Puska M J, Šob M, Brauer G and Korhonen T 1994 *Phys. Rev.* B **49** 10 947
[19] Tan K E, Bratkovsky A M, Harris R M, Horsfield A P, Nguyen-Manh D, Pettifor D G and Sutton A P 1997 *Modelling Simul. Mater. Sci. Eng.* **5** 187
[20] Hugosson H W, Korzhavyi P, Jansson U, Johansson B and Eriksson O 2001 *Phys. Rev.* B **63** 165116
[21] Eibler R 1993 *J. Phys.: Condens. Matter* **5** 5261
[22] Eibler R 1998 *J. Phys.: Condens. Matter* **10** 10 223
[23] Parthé E and Yvon K 1970 *Acta Crystallogr.* B **26** 153
[24] Bell P S and Lewis M H 1971 *Phil. Mag.* **24** 1247
[25] Moisy-Maurice V, Lorenzelli N, de Novion C H and Convert P 1982 *Acta Metall.* **30** 1769
[26] Wanjara P, Drew R A L, Root J and Yue S 2000 *Acta Mater.* **48** 1443
[27] Tsurekawa S and Yoshinaga H 1992 *J. Japan. Inst. Met.* **56** 133
[28] Em V T and Tashmetov M Yu 1996 *Phys. Status Solidi* b **198** 571
[29] Khaenko B V, Galab S Y and Arbuzov M P 1980 *Sov. Phys.–Crystallogr.* **25** 63
[30] Wimmer E, Krakauer H, Weinert M and Freeman A J 1981 *Phys. Rev.* B **24** 864
Jansen H and Freeman A J 1984 *Phys. Rev.* B **30** 561
[31] Hedin L and Lundqvist S 1972 *J. Physique Coll.* **33** C3 73
[32] Lehmann G and Taut M 1972 *Phys. Status Solidi* **54** 469
Jepsen O and Andersen O K 1971 *Solid State Commun.* **9** 1763
[33] Birch F 1978 *J. Geophys. Res.* **83** 1257
[34] Moisy-Maurice V, de Novion C H, Christensen A N and Just W 1981 *Solid State Commun.* **39** 661
[35] Priem T, Beuneu B, de Novion C H, Chevrier J, Livet J F and Finel A 1988 *Physica* B **156–7** 47
[36] Moisy-Maurice V and de Novion C H 1988 *J. Physique* **49** 1737
[37] Čapkova P and Skala L 1992 *Phys. Status Solidi* b **171** 85
[38] Lobier G and Marcon J P 1969 *C. R. Acad. Sci., Paris* C **268** 1132
[39] Holmberg B 1962 *Acta Chem. Scand.* **16** 1255
[40] Holliday J E 1970 *Advances in X-Ray Analysis* vol 1, ed B L Henke, J B Newkirt and G R Mallet (New York: Plenum) p 136
[41] Häglund J, Grimvall G, Jarlborg T and Fernández Guillermet A 1991 *Phys. Rev.* B **43** 14 400
[42] Fernández Guillermet A and Grimvall G 1992 *J. Phys. Chem. Solids* **53** 105
[43] Chang R and Graham L J 1996 *J. Appl. Phys.* **37** 3778
[44] Wolf W, Podloucky R, Anstretter T and Fischer F D 1999 *Phil. Mag.* B **79** 839
[45] Marksteiner P, Weinberger P, Neckel A, Zeller R and Dederichs P H 1986 *Phys. Rev.* B **33** 812
[46] Schlapansky F, Herzig P, Eibler R, Hobiger G and Neckel A 1989 *Z. Phys.* B **75** 187